Geochemical characterization (REE, Nd and Pb isotopes) of atmospheric mineral dust deposited in two maritime peat bogs from the St. Lawrence North Shore (eastern Canada)

Steve Pratte, François de Vleeschouwer, Michelle Garneau

GEOCHEMICAL CHARACTERIZATION (REE, ND AND PB ISOTOPES) OF ATMOSPHERIC MINERAL DUST DEPOSITED IN TWO MARITIME PEAT BOGS FROM THE ST. LAWRENCE NORTH SHORE (EASTERN CANADA)

Steve Pratte[a,b*], François De Vleeschouwer[b] and Michelle Garneau[a]

[a] GEOTOP, Université du Québec à Montréal, C.P. 8888 Succursale Centre-Ville, Montreal, Canada

[b] ECOLAB, Université de Toulouse, CNRS, INPT, UPS, France

ABSTRACT

Dust deposited on two ombrotrophic peat bogs (Baie and IDH bogs) of the St. Lawrence Gulf and Estuary north shore was geochemically characterized using REE concentrations, Nd and Pb isotopes along with particle grain size. Both cores display similar εNd values, which suggests either a common source or sources with similar signatures in both regions. Combining Nd isotope data with REE patterns and particle size allowed for better insights into the source of deposited dust and the inference of past environmental and climatic conditions in both regions. REE elements, εNd and grain-size distribution suggest that, over the last 2000 years, the Baie bog received more local dust due to increased local storminess in response to regional hydroclimatic instability and temperature variations mainly controlled by solar activity. The same phenomenon occurred in the IDH bog since 620 cal a BP, i.e. during the Little Ice Age, where hydroclimatic and paleoecological changes have been previously documented. While the dust reconstructions and regional climatic records agree relatively well, the discrepancies between paleodust records highlight the complex and variable structure of late Holocene changes in paleoclimate and more particularly past dust deposition in eastern Canada.

0.1 Introduction

Mineral dust plays a complex role in the climate system acting both as a factor affecting climate and as a function of it. For instance, mineral dust has effects on radiative budgets, chemical processes in the atmosphere and on the biogeochemical cycles of many elements (Goudie and Middleton, 2001; Meskhidze *et al.*, 2003). Reconstruction of past dust composition and fluxes is important in order to increase our understanding of Holocene climate variability and biogeochemical cycles, hence, a greater number of paleo-dust studies are required.

Until recently, paleo-dust studies have mainly focused on ice cores (Gabrielli *et al.*, 2010) and marine sediments (deMenocal *et al.*, 2000), while continental records focused mainly on loess deposits (Muhs, 2013). Similarly to ice cores, ombrotrophic peatlands (peat bogs) are fed exclusively by atmospheric deposition (Chambers and Charman, 2004) and can therefore provide reliable records of changes in aerosol composition over time (De Vleeschouwer *et al.*, 2014). These archives present two main advantages in comparison to ice cores: they are ubiquitous at middle to high latitudes and they are easy to date. The potential of peat bogs for the reconstruction of Holocene climate variability through the use of multiple indicators is well established (de Jong *et al.*, 2010 and references therein). Peat bogs are increasingly being used as archive of atmospheric dust deposition (Allan *et al.*, 2013; De Vleeschouwer *et al.*, 2012; Shotyk *et al.*, 2002; Vanneste *et al.*, 2015).

Rare earth elements (REE) inherit the chemical signature of their source rock during weathering and their relative patterns are not significantly affected by physical and chemical processes during transport (McLennan, 1989). Hence, REE have been used as tracers and reference elements in a broad range of environmental studies (Aubert *et al.*, 2006; Chiarenzelli *et al.*, 2001; Greaves, Elderfield and Sholkovitz, 1999). Radiogenic isotope signatures of sediments, namely Nd and Pb, have also been used as a tool to trace the dust source as their isotopic ratios are unaffected by erosion and transport. For example, Biscaye *et al.* (1997) used Nd isotopes in combination with Pb and Sr isotopes to show that Asian desert areas were the main source of soil dust deposited over the Greenland ice sheet during the Pleistocene. Peat bog records of temporal variability of REE and Nd isotopes are still limited to a few sites but proved efficient in dust source tracing (Allan *et al.*, 2013; Aubert *et al.*, 2006; Le Roux *et al.*, 2012; Vanneste *et al.*, 2015). For example, using a combination of dust flux and Nd isotope composition, Le Roux *et*

al. (2012) demonstrated the importance of Saharan dust as a source over Western Europe during the mid-Holocene.

Most dust reconstruction studies focus on arid regions whereas the higher latitudes have been overlooked. To date, few records of terrestrial dust deposition exist in North America (Muhs, 2013; Neff *et al.*, 2008) and consist mainly of loess deposits. Periods of enhanced dust deposition have been identified for the first time in two peat bogs from eastern Canada, although the source of the dust deposited in these records is yet unknown (Pratte, Garneau and De Vleeschouwer, In press). Using a combination of REE concentrations, Nd and Pb isotopes as well as particle size data analysed from the same peat cores, we aimed at 1) characterizing the geochemistry of atmospheric mineral dust deposited in these peat profiles; 2) identifying potential changes in dust sources and 3) evaluating the links between climate variability (e.g. wind strength, direction) and the dust deposited into the peat bogs.

0.2 Material and Methods

0.2.1 Sites description and sampling

The Baie peatland (49°04'N, 68°14'W; 1.5 km^2; 15 m.a.s.l.) is a *Sphagnum*-dominated raised bog located on the Manicouagan delta, along the coast at the eastern end of the Lower St. Lawrence Estuary (Fig. 2.1). More than 4.5 m of peat accumulated over marine silty-clay sediments originating from the Laurentian transgression from 6500-4300 cal a BP (Bernatchez, 2003; Magnan and Garneau, 2014). The peatland is open towards the coast of the St. Lawrence Estuary, where beaches occupy the coastline (700 m from the coring site). Deposits at a higher altitude (> 14 m.a.s.l.), onto which soils developed, consist of silt-sand deltaic terraces emerged following the withdrawal of the Goldthwait Sea from 8 ka (Bernatchez, 2003). The regional bedrock is composed of rocks of Paleoproterozoic and Mesoproterozoic age from the Grenville province, mostly gneisses and granites (Fig. 2.1c).

The Ile du Havre peatland (IDH) (50°13'N, 63°36'W, 0.5 km^2; 31 m.a.s.l.) is a raised bog dominated by *Sphagnum* mosses, Ericaceous shrubs and *Cladina* spp. lichens and surrounded by a tree fringe mainly composed of *Picea mariana*. It is located on a 12-km^2 island, two kilometers offshore in the eastern part of the Mingan archipelago in the Gulf of St. Lawrence (Fig. 2.1). Peat

started to accumulate at *ca* 7800 cal a BP in a depression over silty-clay sediments (Pratte, Garneau and De Vleeschouwer, In press). At its deepest part, peat thickness reaches about 6.25 m. The islands of the archipelago are characterized by cuesta landforms with cliffs to the north and slopes towards the south (Grondin *et al.*, 1980). The peatland being located at the north-east side of the island, the surrounding topography is characterized by cliffs and steep slopes. The coastline of the island (600 m away from the peatland) is dominated by beaches, which compose the main unconsolidated sediments. The underlying bedrock consists of Ordovician limestone intersected by layers of shale and sandstone from the Mingan formation (Grondin *et al.*, 1980; Poole *et al.*, 1970).

A core was retrieved from the deepest part of each peatland, using a stainless steel Box corer (10x10 cm cross-section; Jeglum *et al.*, 1992) to sample the upper meter and a Russian sampler (7.5 cm diameter; Jowsey, 1966) for the deeper peat sections. The cores were collected from two holes approximately 30 cm apart in an overlapping manner to ensure complete stratigraphic recovery (see De Vleeschouwer, Chambers and Swindles, 2010 for more details). The cores were wrapped in plastic film, transferred into PVC tubes and stored in a freezer (-20°C) until they were sliced frozen at 1-cm interval (Givelet *et al.*, 2004) using a stainless steel band saw at Ecolab (Toulouse, France).

Bottom sediment samples, from underneath the peatlands, as well as unconsolidated sediments, mineral soils (around Baie bog) and rocks from the surrounding areas (< 10 km) of both study sites were collected (n = 10). The < 63 µm fraction of unconsolidated sediment and soil samples was dried and ground while rocks were cut and fresh material ground.

0.2.2 Chronological control

The construction of the age-depth models for both cores is described in detail in Pratte, Garneau and De Vleeschouwer (In press). In brief, the chronology was constrained by ^{210}Pb activities measured in the uppermost layers of peat (35 and 52 cm for Baie and IDH respectively) by alpha spectrometry at GEOTOP Research center (UQAM, Montreal) and 25 ^{14}C AMS dates (13 and 11 for Baie and IDH respectively) on extracted aboveground plant macrofossils. The ^{14}C dates were processed at Keck-CCAMS facility (Irvine, USA). The constant rate of supply model was

applied to derive ^{210}Pb ages of the upper part of the cores (Appleby, 2002). The measurement uncertainties (Tables 2.2 and 2.3), corresponding to one-sigma, were calculated from counting statistics. The atmospheric, or excess ($^{210}Pb_{ex}$), is used to determine the chronology of environmental records. Supported ^{210}Pb activity, i.e. produced *in situ*, was estimated by the analysis of deeper samples in each core in order to determine at which depth the $^{210}Pb_{ex}$ was not present anymore, hence the limit of the dating technique (Le Roux and Marshall, 2011). Age-depth models were generated by combining both ^{14}C and ^{210}Pb dates using the *BACON* software package (Blaauw and Christen, 2011).

0.2.3 Grain-size analyses

Grain-size distribution was determined on the water-insoluble fraction of the bulk peat samples using a Horiba LA-950 laser grain-size analyzer at Ecolab (Toulouse, France). This instrument measures the volume percent of selected bin-size ranges in samples from 0.1 to 3000 µm. Prior to analyses, peat sample were ashed at 550°C for 6h in a muffle furnace. Samples were soaked in deionized water to dissolve potential pseudo-minerals (salts) formed during ashing, and submitted to ultrasounds to separate particles. A number of samples (up to 4 cm) were combined to provide enough material for analyses. The grain-size distribution of the samples was characterized in 70 classes.

0.2.4 Elemental analyses

All geochemical sample preparations were performed under clean laboratory conditions (class 100) using acid-cleaned labware. Approximately 100 mg of powdered peat samples were acid-digested until complete dissolution, using a series of steps (HNO_3 + HF, then H_2O_2) in Savillex® beakers on a hot plate (Le Roux and De Vleeschouwer, 2010). In a number of samples, an additional step involving *aqua regia* was necessary to fully digest the organic matter. The sediments, soil fractions and rock samples were acid digested using a mixture of HNO3 + HF, then HCl on a hot plate (Stevenson, Meng and Hillaire-Marcel, 2008). The major elements (Al and Ti) were analyzed by ICP-OES at Ecolab (Toulouse, France) on a Thermo Electron IRIS Intrepid II. The trace elements (Zr, Sc, Pb and REE) concentrations were measured on an Agilent

Technologies 7500ce Q-ICP-MS at *Observatoire Midi-Pyrénées* (Toulouse, France). Prior to ICP-MS analyses, samples were diluted and an In-Re spike was added for internal normalization process.

The analytical performance was monitored through reference materials (NIST 1515 Apple leaves, NIST 1547 Peach leaves, NIST 1575a Pine needles, GBW07604 Bush branches and leaves, and NIMT/UOE/FM/001 peat). Measurements performed by ICP-OES were generally within 10% of certified values with the exception of Al concentrations which accuracy was between 6 and 17%. The elements measured by ICP-MS were all within 15% of certified values with the exception of Ce (16%) and Lu (19%). The reproducibility of the digestion procedure was evaluated by repeated analyses of NIST 1515 (n = 5), NIST 1547 (n = 5), GBW-07063 (n = 4) and 10 peat samples (each n = 2) and was generally better than 20%. The procedural blanks for the element analyzed were <15 ppt for trace elements and <1 ppm for Al and Ti.

0.2.5 Pb isotopes

After measurement of Pb concentrations, a series of selected sample mother solutions were diluted to 500 µg g^{-1} for analyses by HR-ICP-MS at the *Observatoire Midi-Pyrénées* (Toulouse, France) (Krachler *et al.*, 2004). Mass bias was controlled and corrected by standard bracketing of a 500 µg g^{-1} standard solution of SRM 981 between each sample. The $^{206}Pb/^{207}Pb$ ratios obtained for the NIMT peat standard were 1.1772 ± 0.0007 compared to the reported value of 1.1763 ± 0.0004 (Yafa *et al.*, 2004).

0.2.6 Nd isotopes

Peat, rock, unconsolidated sediment and soil samples were prepared for Nd isotopes. Between 100 and 600 mg of dried peat (100 mg for the soil/sediment samples) was placed in oven at 550°C for 6 h, to remove all organic matter by combustion (Chambers, Beilman and Yu, 2011). The resulting ashes were acid-digested in a mixture of 16N HNO_3 and 23N HF in a proportion of 1:4 on a hot plate at 125°C for 48h. To ensure complete dissolution, the residues were re-dissolved in 2 ml of 6N HCl. Residues were dissolved into 1N HNO_3 and Nd was purified by a

passage through two sets of columns. Alkalis (e.g. Ca, Rb, Sr) and REE were separated by a passage through Bio-Rad columns filled with pre-conditioned TRU Spec© resin (50-100 mesh) using dilute HNO_3 (0.05N). This solution was directly loaded onto pre-conditioned and pre-calibrated LN Spec© columns and Nd was isolated sequentially from the other REE using dilute HCl (0.2N). The Nd solution was evaporated and dissolved another time in 2% HNO_3 prior to Nd isotopic measurements.

The Nd isotopic measurements were performed using a MC-ICP-MS (multi-collector inductively coupled plasma mass spectrometer, Nu Plasma II) a GEOTOP-UQAM, in Montreal. Replicate analysis of the JNDi-1 Nd standard (Tanaka *et al.*, 2000) every five samples yielded a $^{143}Nd/^{144}Nd$ value of 0.512084 ± 0.000014 (2σ, n = 16). Mass fractionation was corrected to $^{146}Nd/^{144}Nd$ = 0.7219. Epsilon neodymium (εNd) was calculated according to DePaolo and Wasserburg (1976):

$$\varepsilon\mathrm{Nd} = \left(\frac{\left(\frac{143Nd}{144Nd}\right)}{0.512638} - 1 \right) * 10000$$

where 0.512638 corresponds to the chondritic uniform reservoir (CHUR) and represents present-day average earth value (Jacobsen and Wasserburg, 1980).

0.3 Results

0.3.1 Chronology

The results for radiocarbon measurements are presented in Table 2.1, while ^{210}Pb activity and CRS-models are presented in Tables 2.2 and 2.3 for the Baie and IDH cores respectively. Complete details for the measurements and age models are reported in Pratte, Garneau and De Vleeschouwer (In press). Three periods with different accumulation rates were reconstructed in the Baie core (Fig. 2.2). Most of the core shows a relatively constant accumulation rate, with an

average of 1.0 mm a^{-1} from the base to 52-cm depth (4400-400 cal a BP). A second period with lower accumulation rates is found between 52 and 32 cm (400-25 cal a BP: 0.4 mm a^{-1}) while the section between 32 cm and the surface displays values of 2-5 mm a^{-1} and corresponds to the acrotelm, which is composed of poorly decomposed peat and living mosses. In the IDH core, five distinct periods of peat accumulation were identified. From the base of the core to 554 cm (0.5 mm a^{-1}; 7100-5780 cal a BP), from 554 to 452 cm (1.1 mm a^{-1}; 5780-4880 cal a BP), between 452 and 143 cm (0.8 mm a^{-1}; 4880-870 cal a BP), from 143 cm to 45 cm (1.2 mm a^{-1}; 870-35 cal a BP) and from 45 cm to the surface (3-5 mm a^{-1}; 35 cal a BP to present-day), which corresponds to the acrotelm.

0.3.2 Grain-size analyses

The grain-size distribution in the Baie and IDH records are shown in Fig. 2.3. In the Baie record, particles of silt size (2-63 µm) dominate while varying amounts of clay (< 2 µm) and sand (63 µm – 2 mm) particles are present. A relatively constant grain-size distribution is observed during the period 4400-2900 cal a BP (Fig. 2.3), with a median grain-size varying between 7.5 and 11 µm. The median grain-size decreases to an average close to 2 µm between 2820 and 2640 cal a BP. Afterwards, a greater variability in the grain-size distribution is apparent with the occurrence of clays and very fine silts, for short periods of time, and several "peaks" in grain size, displaying distributions that are less well-sorted (Fig. 2.3). The peat layer at 29.7 cm (-5 cal a BP) of depth has a high volume of sand-size particles.

The grain-size distribution in the IDH record is also dominated by silt particles, but there are more clay-sized particles and less sand-sized particles than in the Baie record. From the bottom of the core until 5000 cal a BP, which represents the fen (minerotrophic) section up to the fen-to-bog transition, the IDH core displays coarser grain-size distribution than the rest of the profile (Fig. 2.3). From 5000 to 4000 cal a BP, the median grain size ranges from 1.2 to 2.9 µm, while it shows more variability with values of 1.5-5.8 µm between 4000-2100 cal a BP. The grain-size decreases to values of 0.5-3 µm between 2100-1500 cal a BP. From 1500 cal a BP towards the surface, the grain size of dust varies considerably with values ranging between 2.3 and 10 µm.

The peat layer at 40.1 cm (110 cal a BP), is characterized by the presence of sand particles up to 2 mm.

0.3.3 REE content

All REE display similar depth profiles in each core and vary in parallel with other lithogenic elements such as Ti or Zr. This similar chemical behaviour was confirmed by PCA analyses performed on the elemental profiles in both cores (Pratte, Garneau and De Vleeschouwer, In press). Lanthanum content ranges between 0.07 and 8.2 µg g^{-1} in the Baie core, while it ranges between 0.05 and 19.8 µg g^{-1} in the IDH core (Fig. 2.4). In both cores, the highest REE concentrations and ΣREE/Ti ratios are found at the base, in the minerotrophic and fen-to-bog transition (FBT) sections (455-380 cm in Baie and 623-500 cm in IDH). Individual REE profiles decrease gradually up to 435 cm and 500 cm of depth in the Baie and IDH cores, respectively. In the Baie core, REE concentrations and La/Sm ratios remain relatively low and constant between 435 and 235 cm (4300-2600 cal a BP) as well as between 112 and 70 cm (1075-640 cal a BP). They increase two- to fivefold, between 235 and 112 cm (2600-1075 cal a BP) and up to tenfold from 70 to 25 cm (640 to -25 cal a BP), while La/Sm ratios remain around 0.9 for the former and increase to values near 1.4 in the latter sections.

In the IDH core, apart from two periods when REE concentrations increased threefold between 413-313 cm (4170-2830 cal a BP) and 67-25 cm (1750 to -20 cal a BP), most of the REE concentrations are low and constant (Fig. 2.4). These changes in REE concentrations are not reflected in the profiles of ΣREE/Ti and La/Sm ratios as they display small variability throughout the ombrotrophic section (500-20 cm). From 20 cm depth to the surface, the ΣREE/Ti ratios decrease gradually.

0.3.4 Nd and Pb isotopes

The εNd values range between -12.6 and -22.3 and from -11.8 to -21.0 in the Baie and IDH cores respectively, while the $^{206}Pb/^{207}Pb$ ratios vary between 1.168 and 1.215 in the Baie core and 1.122 and 1.253 in the IDH core (Tables 2.4 and 2.5). Bottom sediments at the base of each core

yielded εNd values of -21.3 and -19.2 and $^{206}Pb/^{207}Pb$ values of 1.123 and 1.138 in Baie and IDH respectively. Epsilon Nd values in the Baie core are at their highest (less negative) between 390 and 225 cm (4000-2500 cal a BP), with εNd of -12.6 to -13.3, while $^{206}Pb/^{207}Pb$ ratios of 1.201-1.215 are observed (Fig. 2.4). From 225 cm to the top of the core (2000 cal a BP to present-day), εNd values show more variability and more negative values (between –13.4 and -15.2). The $^{206}Pb/^{207}Pb$ ratios also display slightly more variability than the preceding period with ratios ranging between 1.188 and 1.206. Over the last 100 years, the $^{206}Pb/^{207}Pb$ ratios decrease to reach their minimum value of 1.168 near the surface.

The minerotrophic section of the IDH core has the most negative εNd values. At the base, εNd values reach -21.3 at 620 cm (6975 cal a BP) and they increase towards the fen-to-bog transition, reaching -17.9 at 500 cm (5330 cal a BP) (Fig. 2.4). A second section of the core from 470 to 111 cm (5050-620 cal a BP) shows relatively stable εNd values ranging between -11.8 and -12.5 with a level (290.7 cm) yielding a value of -13.2. From 111 cm towards the surface (620 cal a BP to the present-day), the εNd values decrease and display slightly more variability with values between -12.8 and -15.1. A similar trend is observed for the $^{206}Pb/^{207}Pb$ ratios, i.e. less radiogenic ratios in the minerotrophic section (1.12) with a gradual increase towards the FBT (1.18-1.20). Stable $^{206}Pb/^{207}Pb$ ratios (1.193-1.208) are also observed between 5330 and 620 cal a BP. A sample at 67.1cm of depth (200 cal a BP) yielded a ratio of 1.25. Afterwards, $^{206}Pb/^{207}Pb$ ratios decrease towards the surface to reach a minimum of 1.167.

0.4 Discussion

0.4.1 REE distribution patterns

The REE content of peat samples and surrounding soils, unconsolidated sediments and rocks, normalized to the Upper Continental Crust (UCC; Wedepohl, 1995), are shown in Fig. 2.5. Both Baie and IDH peat bogs have relatively homogeneous crustal-normalized REE patterns. In the vicinity of the Baie bog, unconsolidated sediments from the beach are characterized by a flat pattern without Eu anomaly. On the other hand, deltaic deposits, onto which soils developed, display slightly higher HREE content and positive Eu anomaly (Fig. 2.5). In the Baie bog, the samples in the fen section (447-435 cm) have a negative Eu anomaly and lower HREE than

LREE, when compared to the FBT (435-380 cm) and bog samples (380 cm to the surface). This can be explained by the contribution from the bottom mineral sediments and local rocks such as gneisses. The other samples (FBT and bog) display an increasing influence of local sediments/soils with less negative (FBT) or no Eu anomaly (bog). The REE patterns in the bog section reflect a mixture of particles from the local soils and the beach. Over the last 1700 years, some samples (Fig. 2.5; Baie 'events') received a greater proportion of particles from the local soil as shown by the positive Eu anomaly. A greater number of these samples is found over the last 600 years, which comprises the Little Ice Age (LIA) period.

The REE for the local beach near IDH peatland show a flat pattern with a slight negative Eu anomaly and enrichment in HREE, while the limestone also displays a negative Eu anomaly along with a MREE and HREE enrichment (Fig. 2.5). Peat samples from the fen section (624-605 cm) have a negative Eu anomaly with an enrichment in LREE. This reflects the contribution from the bottom sediments and the local limestone. The rather flat patterns of the FBT (605-523 cm) and bog (523 cm-surface) samples reflect the increasing proportion of particles from the beach over the bottom sediments.

0.4.2 Dust sources

As mentioned previously, REE in the ombrotrophic section of each core vary in parallel with conservative elements such as Ti, Zr or Al (Pratte, Garneau and De Vleeschouwer, In press), which confirms that REE are immobile and preserved in the peat column, therefore their concentrations are controlled by atmospheric deposition from local and/or regional sources (Aubert *et al.*, 2006; Kylander *et al.*, 2007).

Usually, the REE composition and isotopic signature of dust is inherited from its source rock, allowing its fingerprinting (Aubert *et al.*, 2006; Grousset and Biscaye, 2005; Kylander *et al.*, 2007). To identify the origin of the dust deposited in Baie and IDH bogs, all peat samples and potential local and regional sources were plotted on a $^{206}Pb/^{207}Pb$ vs εNd diagram (Fig. 2.6). The εNd exhibits a wide range in both cores, between -22 and -12, which suggests contrasting sources over the studied period. Figure 2.6 shows that samples from the minerotrophic and FBT have lower εNd (-22 to -17 and -21 to -17 in Baie and IDH respectively) and $^{206}Pb/^{207}Pb$ (1.12-

1.17 for Baie and 1.12-1.18 for IDH) signatures. The lower εNd values in the fen section of each core is linked with a significant enrichment in Nd content (Fig. 2.7). This is in agreement with the εNd values obtained from bottom sediments of Baie (-21) and IDH (-19) as well as the grain-size distribution, which shows the presence of larger particles unlikely to have been transported over long distance (Fig. 2.3). The bottom sediments at both sites represent a mixture of several sources that likely explains the variability of the εNd of both fen sections. In the vicinity of Baie bog, soils that developed over deltaic sediments, and beach sands exhibit εNd values of -17 and -19 respectively, while sandy beach sediments around IDH display a value of -19.

The ombrotrophic sections of the Baie and IDH cores, which received particles of atmospheric origin only, possess a similar range of εNd and $^{206}Pb/^{207}Pb$ values (Fig. 2.6), although the εNd values for IDH are slightly less negative (-11.8 to -13.1) than Baie (-12.6 to -15) before 650 cal a BP. The overlapping εNd values of both cores with those from the Appalachians (Fagel *et al.*, 2002) and St. Lawrence Gulf sediments (Farmer, Barber and Andrews, 2003) could be explained by a common source for particles deposited in each peatland. More likely, the similar εNd values in both cores could be explained by regional sources with similar Nd isotopic ratios as suggested by the fact that rocks in each region display similar εNd values (Dickin, 2000; Dickin and Higgins, 1992). Similarly, $^{206}Pb/^{207}Pb$ ratios show more radiogenic values over the same period (1.19-1.21) and fall within the range of reported values for natural sources (Gallon *et al.*, 2005; Kylander *et al.*, 2010; Wedepohl, 1995).

The lack of isotopic data for the region and the fact that the currently available data display similar isotopic signatures prevent the identification of single sources for particles being deposited in the Baie and IDH bogs. However, when REE patterns are taken into account with εNd, we can reasonably conclude that the particles deposited on both sites come from a mixture of sources. Local sediments such as soils and beach sands are a likely source, while the similarity of the Gulf of the St. Lawrence sediments, also representing a mixture of sources, and Appalachians εNd signatures, suggest that regional sources also contribute. Futhermore, a shift in the Nd isotopic data is linked with the transition from fen to bog conditions in both cores (Fig. 2.7) suggesting that at least three sources must be invoked to explain the variability in εNd.

The gradual decrease in $^{206}Pb/^{207}Pb$ during the recent years (Fig. 2.4) is due to anthropogenic impacts, likely from leaded gasoline emissions. The isotopic ratios in both cores (1.16-1.17) are in agreement with those obtained from another core in the Baie bog (Pratte, Mucci and Garneau, 2013). Since AD 1950 (20 cm-surface), the ΣREE/Ti have decreased gradually in the IDH core (Fig. 2.4), which suggests a change in the source of the deposited dust in the region. This could be explained by the presence of a Ti mine (Lac Tio mine) and shipping facilities, which started operating in 1950, in the port of Havre-Saint-Pierre, located 2 km north of the study site.

0.4.3 Climate-related changes in the dust signal

The temporal εNd evolution can be used to retrieve information about past climate variations when combined with other proxies. Here, we integrate elemental (in the form of dust flux and REE patterns) and isotopic geochemical data as well as grain size to track past climatic influences registered in both records. To extract the climate signal from dust, REE concentrations were used to derive dust fluxes (Chapter 1: Pratte, Garneau and De Vleeschouwer, In press). Then, the dust-rich events previously identified, were analyzed for Nd isotopic composition and compared with local and regional sources. Finally, these changes are interpreted in terms of local or regional environmental changes.

Based on the εNd record, the Baie bog can be divided into three intervals (Fig. 2.8; B-1: 4400-3800 cal a BP, B-2: 3270-2300 cal a BP and B-3: 2000 cal a BP-present). The interval 4400-3800 cal a BP (zone 1) comprises the minerotrophic phase and hence represents a local signal combining both atmospheric and lateral inputs. The influence of the bottom sediments and local bedrock on the εNd signal decreases towards the FBT as shown by the increasing values (Fig. 2.7 and 2.8). The REE patterns for the fen and FBT phases agree with the εNd signal as it displays a decreasing influence of the bottom sediments and local rocks in favour of particles from local mineral soils and the nearby beach (Fig. 2.5).

The second interval, covering the period of 3270-2600 cal BP (B-2), has the highest εNd values of the record (Fig. 2.8). The dust flux displays a relative stability and the grain size does as well apart for the period of 2800-2600 cal a BP, where it possesses the lowest particle size in the record (Fig. 2.3). In the REE patterns (Fig. 2.5) no distinction can be made between this period

and the following one (last 2000 years). A testate amoebae record from the same bog shows relatively high and constant water-table depth (WTD) over this period, suggesting wetter hydroclimatic conditions (Fig. 2.8; Magnan and Garneau, 2014). A pollen-based reconstruction of July temperature anomaly in Baie peatland reports slightly cooler conditions from 4000 cal a BP (Sauvé, 2016) while Viau and Gajewski (2009) reconstructed warmer but wetter conditions for northern Quebec. We hypothesize that the change in Nd values and particles size reflects more humid and, more importantly, stable conditions, which may have reduced the local dust load in favour of more regional sources, especially during the 2800-2600 cal a BP interval. The REE pattern of the samples over that period reveals that local sources were still contributing to a certain extent.

The interval covering the last 2000 years (B-3) is marked by more negative εNd values, greater and more variable dust flux and particle grain size (Fig. 2.3 and 2.8). The lower εNd values and greater particle size suggest a greater proportion of particles originating from a local source. This is further confirmed by the REE patterns that reflect a mixture between the local mineral soils and the beach (i.e. bog in Fig. 2.5). Although not of the same amplitude as the dust flux, the εNd record for this period displays greater variability. This high variability was also observed in the WTD reconstruction from Magnan and Garneau (2014) (Fig. 2.8). Hydroclimatic instability has been reported to affect dust loads through increased storminess (de Jong, Schoning and Björck, 2007; De Vleeschouwer *et al.*, 2009). Decreasing July temperature anomalies over the last 2000 years also suggest a climatic "deterioration", shortly interrupted around 1.100 cal a BP (Viau and Gajewski, 2009). An agreement between the dust flux record and solar minima (Reimer *et al.*, 2013) was noted for the Baie bog (Pratte, Garneau and De Vleeschouwer, In press). Hence, over the last 2000 years, the dust εNd signature, particle size and flux all point towards increased local storminess, which deposited a greater proportion of particles from local sources in response to regional (hydrology) and global (temperature; i.e. solar minima) events. This is especially true for the last ca 600 years, when distinct events (Fig. 2.8; red lines) with REE patterns closer to the signature of the local soils where recorded (Fig. 2.5).

A closer look at the εNd record of IDH bog reveals three intervals: 7100-5000 cal (I-1) a BP, 5000-620 cal a BP (I-2) and 410 cal a BP to the present day (I-3). The interval 7100-5000 cal a BP (I-1) represents the minerotrophic and FBT sections with values typical for the local sources,

mostly brought to the peatland by lateral inputs. As in the Baie core, the gradual increase in εNd and $^{206}Pb/^{207}Pb$ values towards the top of the minerotrophic section is explained by the gradual isolation of the peat surface from the local runoff and the proportionally increasing importance of atmospheric particles, from sources such as beach sands, on the isotopic signatures (Fig. 2.4, 2.7 and 2.8). This is confirmed by the REE pattern of the FBT transition samples, which has values more similar to the beach than the bottom sediments and limestone (Fig. 2.5).

In the second interval (I-2: 5000-620 cal a BP), the εNd profile mirrors the REE dust flux, i.e. it shows relatively constant values (mean: -12.3±0.3). The grain-size record displays a similar pattern (Fig. 2.3). A WTD record from a core collected 5 km north of IDH bog (Plaine bog) displays large hydrological variations over the same period (Magnan and Garneau, 2014), which are not reflected in any proxy from IDH bog. The geographical setting (on an island, protected by a forest fringe, higher elevation) of the IDH bog was invoked as a factor reducing the amount of dust being deposited on the site and explaining the low dust flux (Pratte, Garneau and De Vleeschouwer, In press). While the "isolation" of IDH probably contributes to the stability of the dust record, it cannot explain alone the εNd values. The nearly constant εNd signal either means that dust has a single source within that timespan or that the εNd values of the surrounding geological formations are not diagnostic. Nevertheless, the similarity of the REE pattern of the peat samples for the period to those of the beach suggests a dominant local source.

The last interval, covering 620 cal a BP to the present (I-3), has more negative εNd values and greater particle size (~10µm) suggesting a greater proportion of local dust sources. While the REE patterns (Fig. 2.5) reveal that atmospheric particles from local source (beach) are an important source, they do not display distinct patterns when compared to the previous period (5000-620 cal a BP). The dust flux increases slightly over the period as well (Fig. 2.8). Reconstructed WTD on the continental shore suggests wetter and colder conditions on the coast (Magnan and Garneau, 2014). Furthermore, Viau and Gajewski (2009) report that northern Quebec was the coldest Canadian region during the LIA. Similarly to the Baie bog, the εNd values and the particles size of the dust deposited onto the IDH bog indicate locally increased wind intensity.

As previously hypothesized, the distinct geographical settings of Baie and IDH bogs might explain the difference in the timing of changes between their records. The changes recorded in the Baie core between 2000 and 1000 cal a BP, might not have been significant enough to be recorded in the IDH site considering its geomorphic setting. Comparatively, changes occurring during the LIA would have been more important, since they were recorded by the IDH record. This is in agreement with what is known about the LIA climatic deterioration, which affected North America on a large scale (Viau and Gajewski, 2009; Wanner *et al.*, 2011). More records from the coast would be needed to verify whether the different dust signal recorded in the IDH bog is representative of the regional dust signal.

0.5 Conclusion

The dust deposited on two peat bogs of the north shore of the Estuary and Gulf of the St. Lawrence was geochemically characterized using REE concentrations, Nd and Pb isotopes. Both cores show distinct REE content, εNd and $^{206}Pb/^{207}Pb$ signatures between minerotrophic and ombrotrophic sections. Baie and IDH bogs display similar εNd values, which either suggests a common source or similar εNd signature for regional sources. While the similar range of εNd values between potential sources prevents a definitive identification of the origin for the dust deposited on both peat bogs, the REE patterns and grain-size distribution reveal that local soils and beach sands are likely sources.

The evolution of the isotopic signal, in combination with the REE patterns, the grain-size distribution and the dust flux, was used to retrieve information on past environmental and climatic conditions in the region. Both sites display signals similar to the bottom sediments and local bedrock during their respective minerotrophic phase, likely overprinting the atmospheric signal. Apart from the minerotrophic phases, the two sites registered two intervals with contrasting εNd values. The IDH bog has a nearly constant εNd signature between 5000 and 620 cal a BP, which suggests a particular source that has not yet been identified. From 3270-2600 cal a BP, the Baie bog shows more regional dust supplies during a more stable climatic phase. The more humid and stable climate reduced particle availability locally in favour of a more regional

signal. REE patterns, grain-size distribution and, to a certain extent, εNd values indicate that a greater proportion of local dust has been deposited over the last 2000 years in the Baie core and the last 600 years in the IDH core, respectively. These inputs are related to increased local storminess (i.e. wind intensity) in response to greater instability in the hydroclimatic conditions on a regional scale and cold events (solar minima) on a more global scale. Over the last century, anthropogenic activities (mining, leaded gasoline) have affected the dust cycle in the region. While these changes agree reasonably well with regional records, the discrepancies between both paleodust records highlight the complex and variable structure of the late-Holocene changes in climate and atmospheric dust.

Acknowledgments

We are grateful to Gaël Le Roux (*Ecolab*, Toulouse), Marie-Jo Tavella (*EcoLab*, Toulouse), David Baqué (*Ecolab*, Toulouse), Aurélie Lanzanova (*Geoscience Environnement Toulouse*), André Poirier (GEOTOP-UQAM, Canada) and Bassam Ghaleb (GEOTOP-UQAM, Canada) for their help with major and trace elements analyses, Nd and Pb isotopes and ^{210}Pb dating. Thanks to Gabriel Magnan, Nicole Sanderson, Antoine Thibault and Hans Asnong for help during fieldwork as well as Julien Gogot for lab assistance. Thanks to *Les Tourbeux* for fruitful discussions. Financial support was provided by Natural Sciences and Engineering Research Council of Canada (NSERC; #250287) discovery grant to MG. Scholarships to SP were provided by the Fonds de Recherche Québec – Nature et Technologie (FRQNT; #176250 and #180723). An additional mobility grant was provided by *Institut National Polytechnique de Toulouse* ("*Soutien à la mobilité*" grant to FDV).

0.6 References

Allan, M., Le Roux, G., Piotrowska, N., Beghin, J., Javaux, E., Court-Picon, M., Mattielli, N., Verheyden, S. and Fagel, N. (2013). Mid and late Holocene dust deposition in western Europe: the Misten peat bog (Hautes Fagnes - Belgium). *Climate of the Past Discussion*, 9(3), 2889-2928.

Appleby, P.G. (2002). Chronostratigraphic Techniques in Recent Sediments. In: Last, W. and J. Smol (dir.), *Tracking Environmental Change Using Lake Sediments* (Vol. 1, p. 171-203): Springer Netherlands.

Aubert, D., Le Roux, G., Krachler, M., Cheburkin, A., Kober, B., Shotyk, W. and Stille, P. (2006). Origin and fluxes of atmospheric REE entering an ombrotrophic peat bog in Black Forest (SW Germany): Evidence from snow, lichens and mosses. *Geochimica et Cosmochimica Acta*, 70(11), 2815-2826.

Bernatchez, P. (2003). *Évolution littorale holocène et actuelle des complexes deltaïques de Betsiamites et Manicouagan-Outardes: synthèse, processus, causes et perspectives.* (PhD). Université Laval, Québec.

Biscaye, P.E., Grousset, F.E., Revel, M., Van der Gaast, S., Zielinski, G.A., Vaars, A. and Kukla, G. (1997). Asian provenance of glacial dust (stage 2) in the Greenland Ice Sheet Project 2 Ice Core, Summit, Greenland. *Journal of Geophysical Research: Oceans*, 102(C12), 26765-26781.

Blaauw, M. and Christen, J.A. (2011). Flexible paleoclimate age-depth models using an autoregressive gamma process. *Bayesian Analysis*, 6, 457-474.

Chambers, F.M. and Charman, D.J. (2004). Holocene environmental change: contributions from the peatland archive. *The Holocene*, 14(1), 1-6.

Chambers, F.M., Beilman, D.W. and Yu, Z.C. (2011). Methods for determining peat humification and for quantifying peat bulk density, organic matter and carbon content for palaeostudies of climate and peatland carbon dynamics. *Mires and Peat*, 7.

Chiarenzelli, J., Aspler, L., Dunn, C., Cousens, B., Ozarko, D. and Powis, K. (2001). Multi-element and rare earth element composition of lichens, mosses, and vascular plants from the Central Barrenlands, Nunavut, Canada. *Applied Geochemistry*, 16(2), 245-270.

de Jong, R., Schoning, K. and Björck, S. (2007). Increased aeolian activity during humidity shifts as recorded in a raised bog in south-west Sweden during the past 1700 years. *Climate of the Past*, 3(3), 411-422.

de Jong, R., Blaauw, M., Chambers, F., Christensen, T., Vleeschouwer, F., Finsinger, W., Fronzek, S., Johansson, M., Kokfelt, U., Lamentowicz, M., Roux, G., Mauquoy, D., Mitchell, E.D., Nichols, J., Samaritani, E. and Geel, B. (2010). Climate and Peatlands. In: Dodson, J. (dir.), *Changing Climates, Earth Systems and Society*: Springer Netherlands.

De Vleeschouwer, F., Piotrowska, N., Sikorski, J., Pawlyta, J., Cheburkin, A., Le Roux, G., Lamentowicz, M., Fagel, N. and Mauquoy, D. (2009). Multiproxy evidence of `Little Ice

Age' palaeoenvironmental changes in a peat bog from northern Poland. *The Holocene*, 19(4), 625-637.

De Vleeschouwer, F., Chambers, F.M. and Swindles, G.T. (2010). Coring and subsampling of peatlands for palaeoenvironmental research. *Mires and Peat*, 7.

De Vleeschouwer, F., Pazdur, A., Luthers, C., Streel, M., Mauquoy, D., Wastiaux, C., Le Roux, G., Moschen, R., Blaauw, M., Pawlyta, J., Sikorski, J. and Piotrowska, N. (2012). A millennial record of environmental change in peat deposits from the Misten bog (East Belgium). *Quaternary International*, 268, 44-57.

De Vleeschouwer, F., Ferrat, M., McGowan, H., Vanneste, H. and Weiss, D. (2014). Extracting paleodust information from peat geochemistry. *PAGES Magazine*, 22(2), 88-89.

deMenocal, P., Ortiz, J., Guilderson, T., Adkins, J., Sarnthein, M., Baker, L. and Yarusinsky, M. (2000). Abrupt onset and termination of the African Humid Period: rapid climate responses to gradual insolation forcing. *Quaternary Science Reviews*, 19(1–5), 347-361.

DePaolo, D.J. and Wasserburg, G.J. (1976). Nd isotopic variations and petrogenetic models. *Geophysical Research Letters*, 3(5), 249-252.

Dickin, A.P. and Higgins, M.D. (1992). Sm/Nd evidence for a major 1.5 Ga crust-forming event in the central Grenville province. *Geology*, 20(2), 137-140.

Dickin, A.P. (2000). Crustal formation in the Grenville Province: Nd-isotope evidence. *Canadian Journal of Earth Sciences*, 37(2-3), 165-181.

Fagel, N., Innocent, C., Gariepy, C. and Hillaire-Marcel, C. (2002). Sources of Labrador Sea sediments since the last glacial maximum inferred from Nd-Pb isotopes. *Geochimica et Cosmochimica Acta*, 66(14), 2569-2581.

Farmer, G.L., Barber, D. and Andrews, J. (2003). Provenance of Late Quaternary ice-proximal sediments in the North Atlantic: Nd, Sr and Pb isotopic evidence. *Earth and Planetary Science Letters*, 209(1–2), 227-243.

Gabrielli, P., Wegner, A., Petit, J.R., Delmonte, B., De Deckker, P., Gaspari, V., Fischer, H., Ruth, U., Kriews, M., Boutron, C., Cescon, P. and Barbante, C. (2010). A major glacial-interglacial change in aeolian dust composition inferred from Rare Earth Elements in Antarctic ice. *Quaternary Science Reviews*, 29(1–2), 265-273.

Gallon, C., Tessier, A., Gobeil, C. and Beaudin, L. (2005). Sources and chronology of atmospheric lead deposition to a Canadian Shield lake: Inferences from Pb isotopes and PAH profiles. *Geochimica et Cosmochimica Acta*, 69(13), 3199-3210.

Givelet, N., Le Roux, G., Cheburkin, A., Chen, B., Frank, J., Goodsite, M.E., Kempter, H., Krachler, M., Noernberg, T., Rausch, N., Rheinberger, S., Roos-Barraclough, F., Sapkota, A., Scholz, C. and Shotyk, W. (2004). Suggested protocol for collecting, handling and preparing peat cores and peat samples for physical, chemical, mineralogical and isotopic analyses. *Journal of Environmental Monitoring*, 6(5), 481-492.

Goudie, A.S. and Middleton, N.J. (2001). Saharan dust storms: nature and consequences. *Earth-Science Reviews*, 56(1–4), 179-204.

Greaves, M.J., Elderfield, H. and Sholkovitz, E.R. (1999). Aeolian sources of rare earth elements to the Western Pacific Ocean. *Marine Chemistry*, 68(1–2), 31-38.

Grousset, F.E. and Biscaye, P.E. (2005). Tracing dust sources and transport patterns using Sr, Nd and Pb isotopes. *Chemical Geology*, 222(3–4), 149-167.

Jacobsen, S.B. and Wasserburg, G.J. (1980). Sm-Nd isotopic evolution of chondrites. *Earth and Planetary Science Letters*, 50(1), 139-155.

Jeglum, JK, Rothwell, RL, Berry, GJ and Smith, G.K.M. (1992). A peat sampler for rapid survey. Technical note, *Canadian Forestry Service* 13: 921–932.

Jowsey PC. (1966) An improved peat sampler. *New Phytologist* 65: 245-248.

Krachler, M., Le Roux, G., Kober, B. and Shotyk, W. (2004). Optimising accuracy and precision of lead isotope measurement (^{206}Pb, ^{207}Pb, ^{208}Pb) in acid digests of peat with ICP-SMS using individual mass discrimination correction. *Journal of Analytical Atomic Spectrometry*, 19(3), 354-361.

Kylander, M.E., Klaminder, J., Bindler, R. and Weiss, D.J. (2010). Natural lead isotope variations in the atmosphere. *Earth and Planetary Science Letters*, 290(1-2), 44-53.

Kylander, M.E., Muller, J., Wüst, R.A.J., Gallagher, K., Garcia-Sanchez, R., Coles, B.J. and Weiss, D.J. (2007). Rare earth element and Pb isotope variations in a 52 kyr peat core from Lynch's Crater (NE Queensland, Australia): Proxy development and application to paleoclimate in the Southern Hemisphere. *Geochimica et Cosmochimica Acta*, 71(4), 942-960.

Le Roux, G. and De Vleeschouwer, F. (2010). Preparation of peat samples for inorganic geochemistry used as palaeoenvironmental proxies. *Mires and Peat*, 7.

Le Roux, G. and Marshall, W.A. (2011). Constructing recent peat accumulation chronologies using atmospheric fall-out radionuclides. *Mires and Peat*, 7.

Le Roux, G., Fagel, N., De Vleeschouwer, F., Krachler, M., Debaille, V., Stille, P., Mattielli, N., van der Knaap, W.O., van Leeuwen, J.F.N. and Shotyk, W. (2012). Volcano- and climate-driven changes in atmospheric dust sources and fluxes since the Late Glacial in Central Europe. *Geology*, 40(4), 335-338.

Magnan, G. and Garneau, M. (2014). Evaluating long-term regional climate variability in the maritime region of the St. Lawrence North Shore (eastern Canada) using a multi-site comparison of peat-based paleohydrological records. *Journal of Quaternary Science*, 29(3), 209-220.

McLennan, S.M. (1989). Rare earth elements in sedimentary rocks; influence of provenance and sedimentary processes. *Reviews in Mineralogy and Geochemistry*, 21(1), 169-200.

Meskhidze, N., Chameides, W.L., Nenes, A. and Chen, G. (2003). Iron mobilization in mineral dust: Can anthropogenic SO2 emissions affect ocean productivity? *Geophysical Research Letters*, 30(21), 2085.

Muhs, D.R. (2013). The geologic records of dust in the Quaternary. *Aeolian Research*, 9, 3-48.

Neff, J.C., Ballantyne, A.P., Farmer, G.L., Mahowald, N.M., Conroy, J.L., Landry, C.C., Overpeck, J.T., Painter, T.H., Lawrence, C.R. and Reynolds, R.L. (2008). Increasing eolian dust deposition in the western United States linked to human activity. *Nature Geoscience*, 1(3), 189-195.

Pratte, S., Garneau, M. and De Vleeschouwer, F. (In press). Late Holocene atmospheric dust deposition in eastern Canada (St. Lawrence North Shore). *The Holocene*

Pratte, S., Mucci, A. and Garneau, M. (2013). Historical records of atmospheric metal deposition along the St. Lawrence Valley (eastern Canada) based on peat bog cores. *Atmospheric Environment*, 79, 831-840.

Reimer, P.J., Bard, E., Bayliss, A., Beck, J.W., Blackwell, P.G., Bronk Ramsey, C., Buck, C.E., Cheng, H., Edwards, R.L., Friedrich, M., Grootes, P.M., Guilderson, T.P., Haflidason, H., Hajdas, I., Hatté, C., Heaton, T.J., Hoffmann, D.L., Hogg, A.G., Hughen, K.A., Kaiser, K.F., Kromer, B., Manning, S.W., Niu, M., Reimer, R.W., Richards, D.A., Scott, E.M., Southon, J.R., Staff, R.A., Turney, C.S.M. and van der Plicht, J. (2013). IntCal13 and

Marine13 Radiocarbon Age Calibration Curves 0–50,000 Years cal BP. *Radiocarbon*, 55(4), 1869-1887.

Shotyk, W., Krachler, M., Martinez-Cortizas, A., Cheburkin, A.K. and Emons, H. (2002). A peat bog record of natural, pre-anthropogenic enrichments of trace elements in atmospheric aerosols since 12 370 ^{14}C yr BP, and their variation with Holocene climate change. *Earth and Planetary Science Letters*, 199(1-2), 21-37.

Stevenson, R.K., Meng, X.W. and Hillaire-Marcel, C. (2008). Impact of melting of the Laurentide Ice Sheet on sediments from the upper continental slope off southeastern Canada: evidence from Sm–Nd isotopes. *Canadian Journal of Earth Sciences*, 45(11), 1243-1252.

Tanaka, T., Togashi, S., Kamioka, H., Amakawa, H., Kagami, H., Hamamoto, T., Yuhara, M., Orihashi, Y., Yoneda, S., Shimizu, H., Kunimaru, T., Takahashi, K., Yanagi, T., Nakano, T., Fujimaki, H., Shinjo, R., Asahara, Y., Tanimizu, M. and Dragusanu, C. (2000). JNdi-1: a neodymium isotopic reference in consistency with LaJolla neodymium. *Chemical Geology*, 168(3–4), 279-281.

Vanneste, H., De Vleeschouwer, F., Martínez-Cortizas, A., von Scheffer, C., Piotrowska, N., Coronato, A. and Le Roux, G. (2015). Late-glacial elevated dust deposition linked to westerly wind shifts in southern South America. *Scientific Reports*, 5

Viau, A.E. and Gajewski, K. (2009). Reconstructing Millennial-Scale, Regional Paleoclimates of Boreal Canada during the Holocene. *Journal of Climate*, 22(2), 316-330.

Wanner, H., Solomina, O., Grosjean, M., Ritz, S.P. and Jetel, M. (2011). Structure and origin of Holocene cold events. *Quaternary Science Reviews*, 30(21–22), 3109-3123.

Wedepohl, K.H. (1995). The composition of the continental crust. *Geochimica et Cosmochimica Acta*, 59(7), 1217-1232.

Yafa, C., Farmer, J.G., Graham, M.C., Bacon, J.R., Barbante, C., Cairns, W.R.L., Bindler, R., Renberg, I., Cheburkin, A., Emons, H., Handley, M.J., Norton, S.A., Krachler, M., Shotyk, W., Li, X.D., Martinez-Cortizas, A., Pulford, I.D., MacIver, V., Schweyer, J., Steinnes, E., Sjobakk, T.E., Weiss, D., Dolgopolova, A. and Kylander, M. (2004). Development of an ombrotrophic peat bog (low ash) reference material for the determination of elemental concentrations. *Journal of Environmental Monitoring*, 6(5), 493-501.

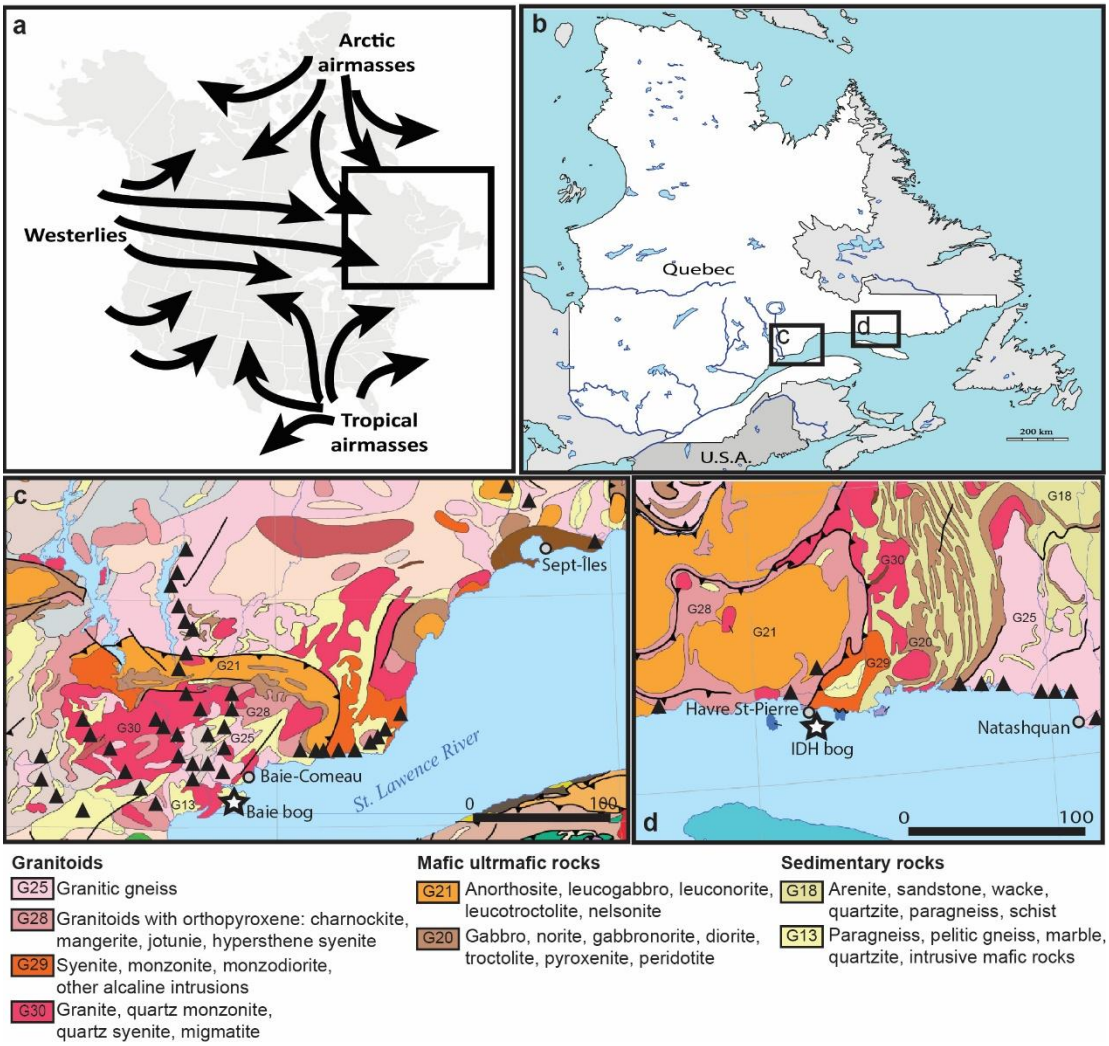

Figure 0.1 Map of the study region : (a) Map of North America showing the main air masses over the region; (b) map of Quebec with the location of the two study areas; (c) location of the Baie bog (star) in the Baie-Comeau region; (d) and location of the IDH bog (star) in the Havre Saint-Pierre region. Grey dots represent towns. Triangles correspond to rock analyzed for $^{143}Nd/^{144}Nd$ by Dickin and Higgins (1992) and Dickin (2000).

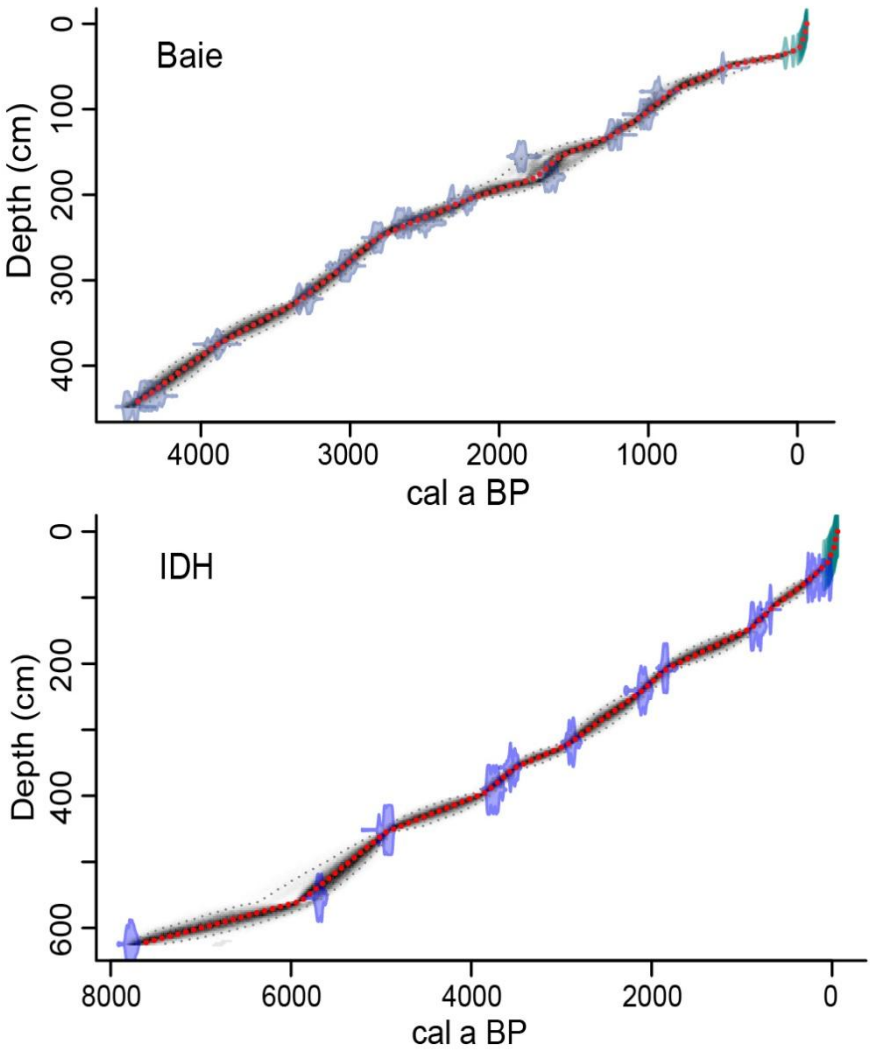

Figure 0.2 Age-depth models for Baie (top) and IDH (bottom) cores constructed using *BACON* software (Blaauw and Christen, 2011) using both ^{210}Pb and ^{14}C dates. The gray bands encompass all possible age-depth models whereas the dotted lines represent the 95% confidence intervals. The red dotted line represents the weighted mean age of each modeled sample. Purple symbols indicate calendar age distribution of ^{14}C dates and light blue symbols show ^{210}Pb ages derived from the CRS model.

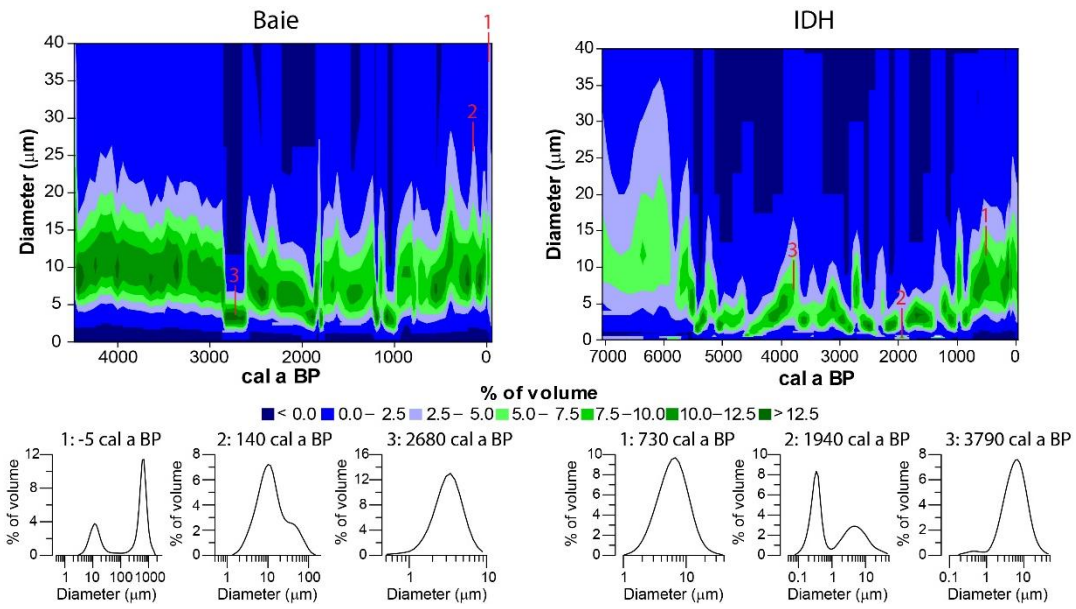

Figure 0.3 Grain-size distribution of water insoluble inorganic fraction from (A) the Baie core and (B) the IDH core. Number 1 to 3 for both core: grain-size distribution of selected samples.

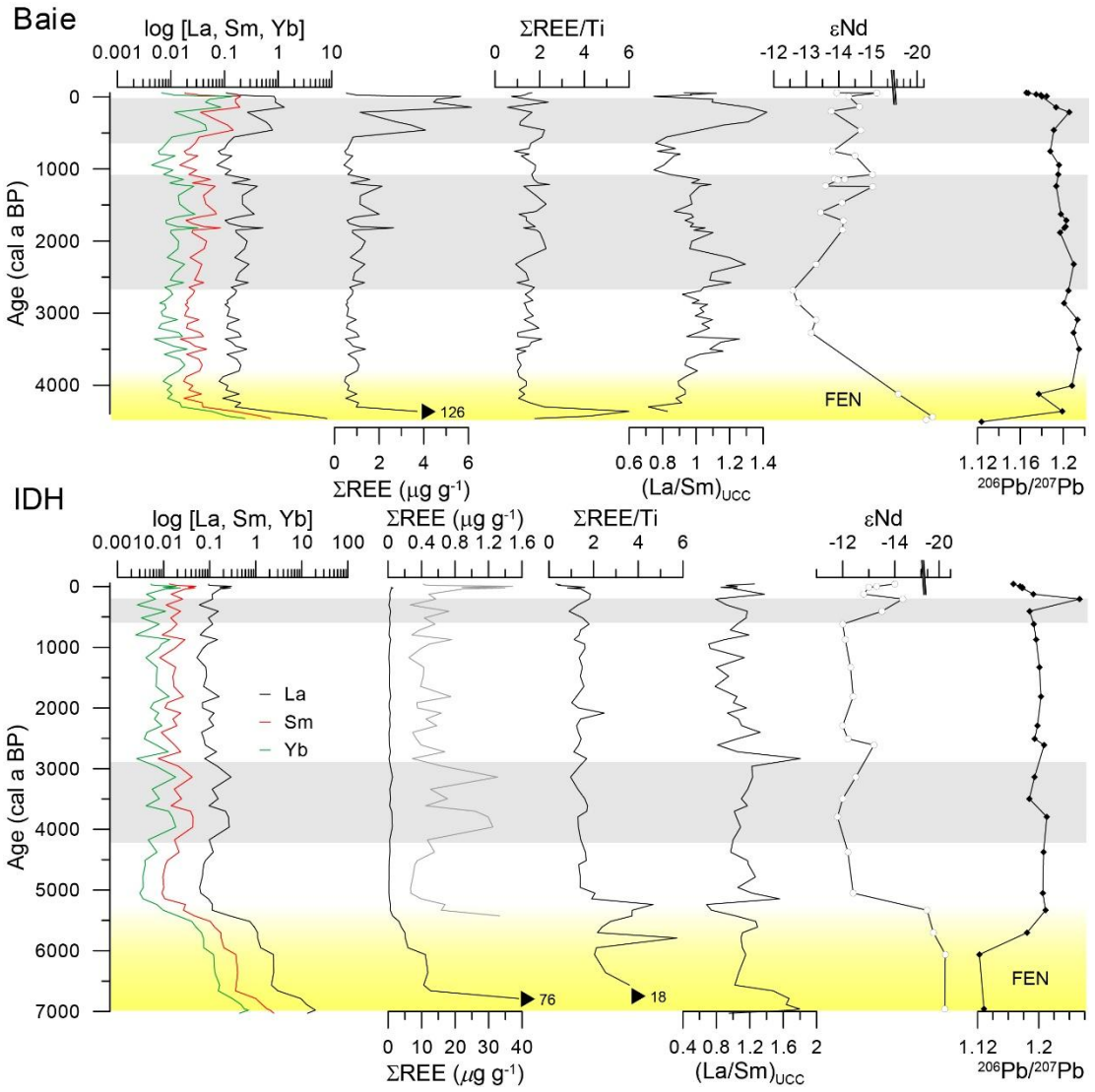

Figure 0.4 La, Sm, Yb (log scale) and ΣREE concentrations, ΣREE/Ti, La/Sm normalized to UCC, εNd and $^{206}Pb/^{207}Pb$ vs. age for Baie (top) and IDH (bottom) cores. Grey areas represent periods of higher elemental concentrations. Yellow areas represent the minerotrophic section (fen) of each core. Black arrows represent maximum values at the bottom of the cores.

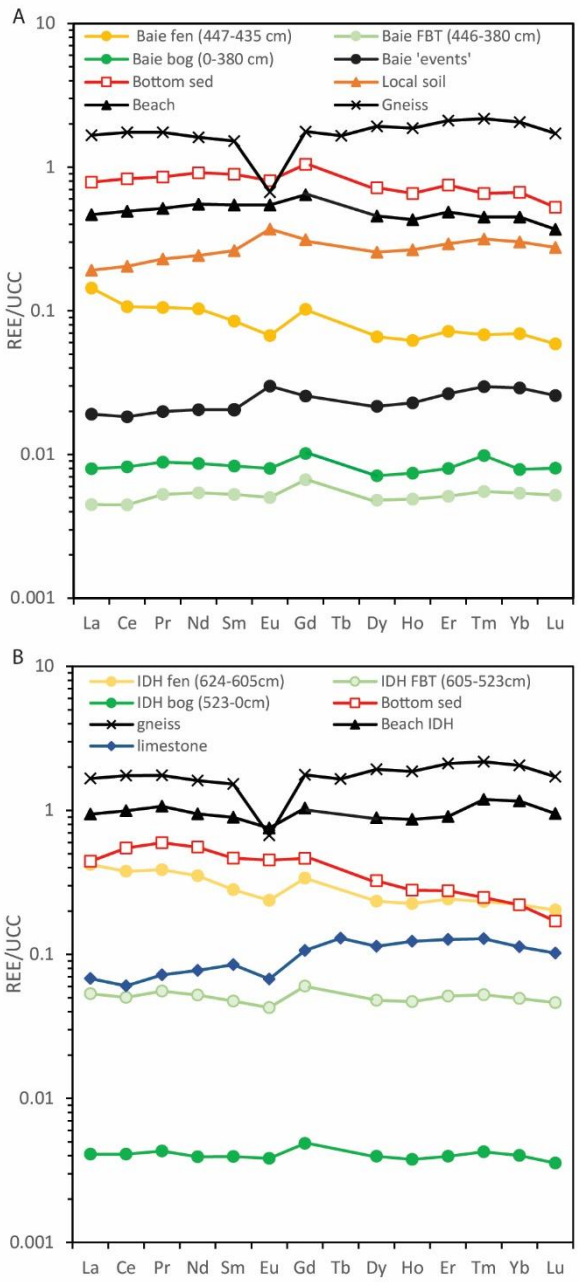

Figure 0.5 UCC-normalized (Wedepohl, 1995) REE patterns for (A) the Baie core and (B) the IDH core. Circles: Mean values for different portion of each core (fen; FBT; bog); squares: basal sediments underneath each core; triangles: local soils and beach; diamonds: limestone; crosses: mean regional gneisses (GEOROC, 2003).

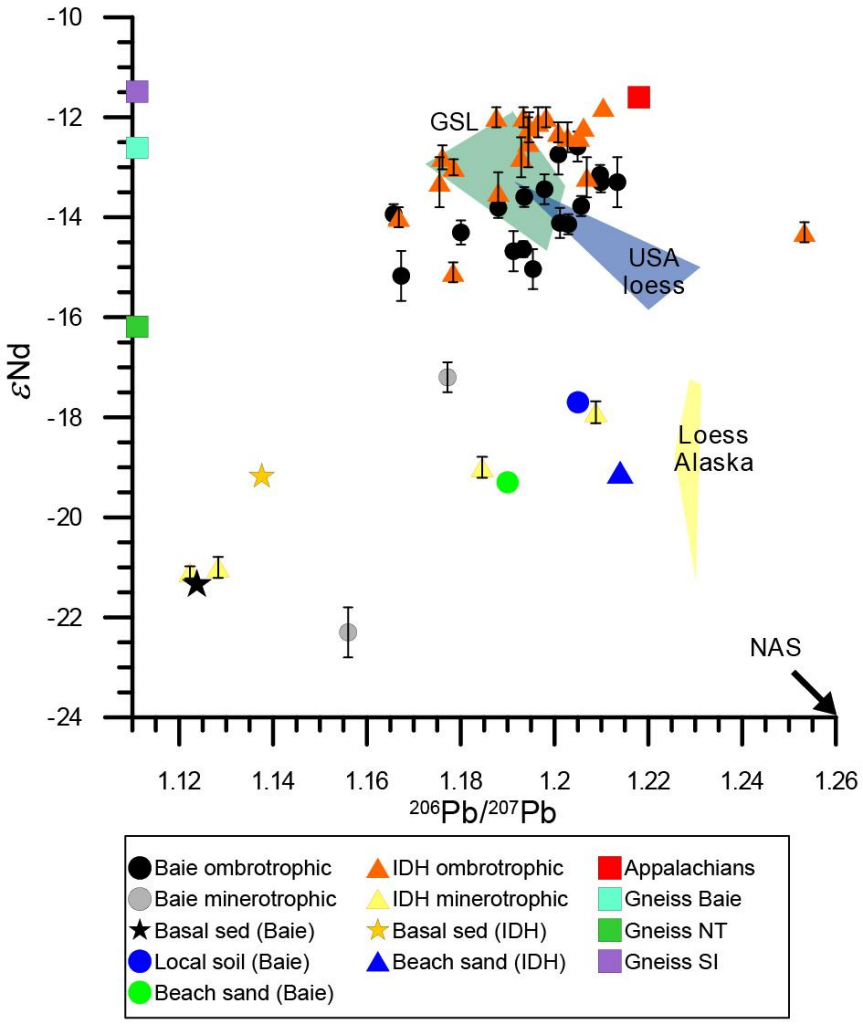

Figure 0.6 εNd vs. $^{206}Pb/^{207}Pb$ for Baie (circles) and IDH (triangles) peat samples. Basal sediments, local soils, beach sand are from this study. Alaskan loess (yellow) and USA loess (blue) areas are from Biscaye *et al.* (1997). Gulf of St. Lawrence samples (GSL; dark green) from Farmer *et al.* (2003) and North American Shield (NAS) from Fagel *et al.* (2002). Squares: potential isotope signature of local (mean gneisses Baie region, Dickin and Higgins (1992); mean gneisses from Sept-Îles (SI) and mean gneisses from Natashquan (NT), Dickin (2000)) and regional (Appalachian (Pan-African crust, Fagel *et al.* (2002). Note that samples with no $^{206}Pb/^{207}Pb$ data are fixed on the left along the y-axis.

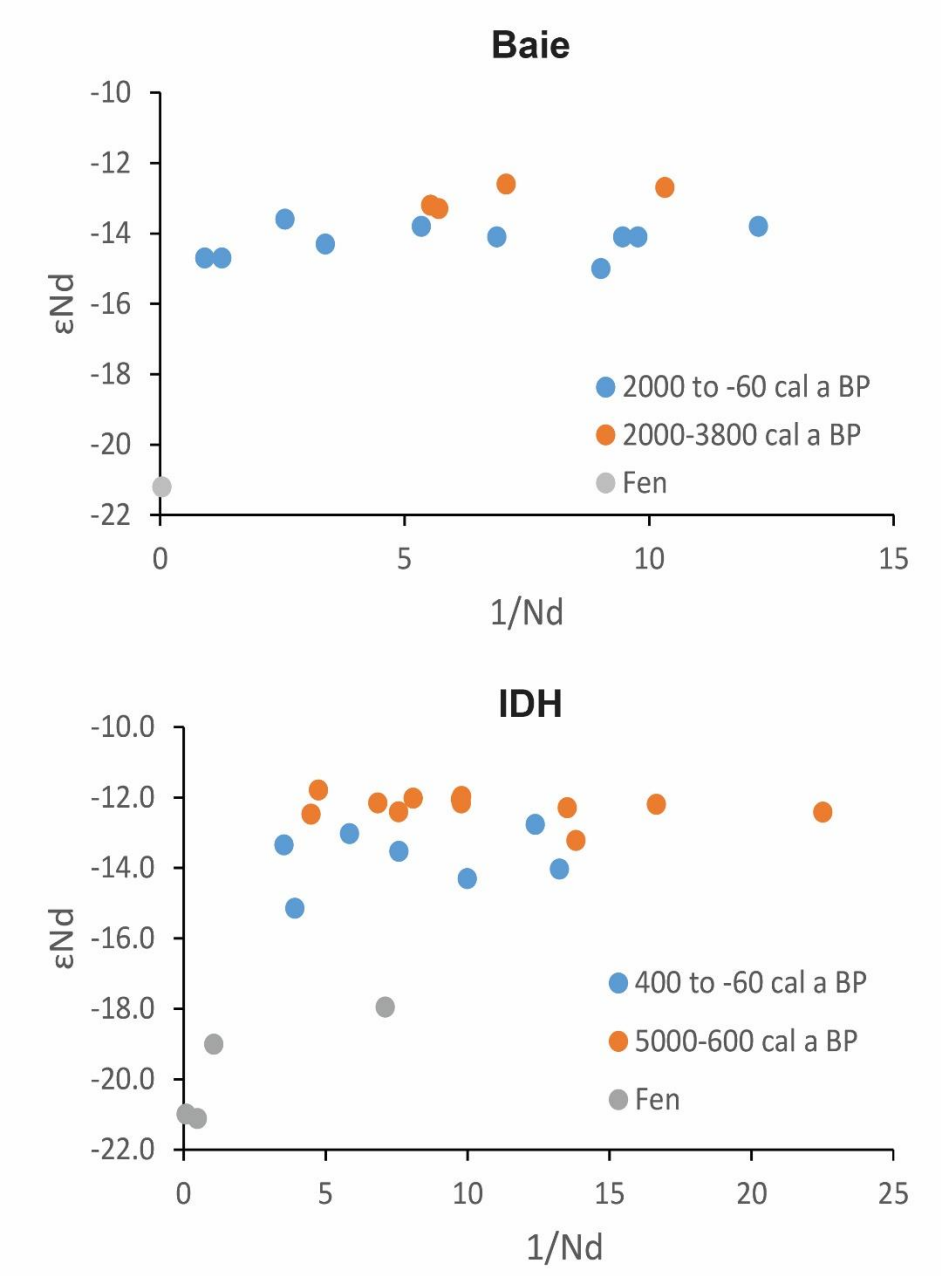

Figure 0.7 Binary diagram of 1/Nd content and εNd for Baie (top) and IDH (bottom) cores.

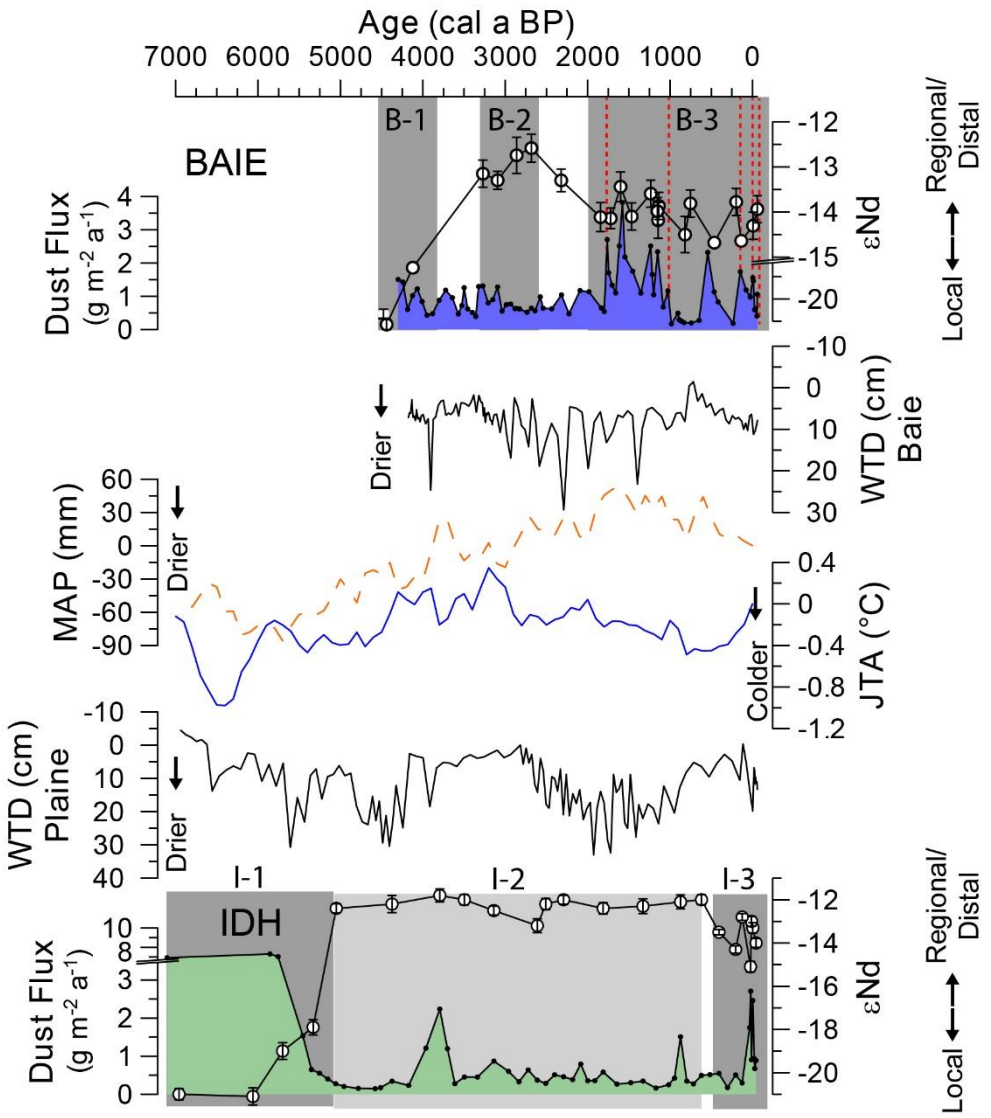

Figure 0.8 Nd isotope composition, evolution of REE-dust flux (Pratte, Garneau and De Vleeschouwer, In press) for Baie (top, blue) and IDH (bottom, green) bogs compared with regional records. Water table depth (WTD) reconstructions for Baie and Plaine are from (Magnan and Garneau, 2014). Mean annual precipitation (MAP; blue dash line) and mean July temperature anomalies (orange) in northern Quebec from Viau and Gajewski (2009). Red dashed lines represent Baie samples with REE patterns closer to local soils (see "Baie events"; Fig. 2.5). Grey areas represents climatic periods discussed in section 2.4.3.

Table 0.1 Results of ^{14}C AMS measurements, calibration and description of samples for Baie and IDH cores.

Site and sample	Depth (cm)	Laboratory number	^{14}C age (BP)	2σ range (cal a BP)	Material dated
Baie					
45	51.6	UCIAMS-129510	425±15	481-513	Charred *Picea mariana* needles
67	79.4	UCIAMS-151367	1015±25	833-971	*Sphagnum* spp. stems
106	105.9	UCIAMS-129511	1120±15	977-1059	*Sphagnum* spp. stems
128	130.0	UCIAMS-129512	1275±15	1181-1271	Charred *Picea mariana* needles
151	155.2	UCIAMS-135384	1905±20	1818-1893	*Sphagnum* spp. stems
173	179.3	UCIAMS-129513	1740±25	1570-1709	*Sphagnum* spp. stems, branches and leaves, charred *Picea mariana* needles
196	206.7	UCIAMS-129514	2250±15	2162-2336	*Sphagnum* spp. stems
217	233.0	UCIAMS-129515	2465±15	2442-2704	*Sphagnum* spp. stems
232	250.2	UCIAMS-129516	2725±15	2779-2853	*Sphagnum* spp. stems
256	283.2	UCIAMS-129517	2900±15	2963-3136	*Sphagnum* spp. stems
286	321.8	UCIAMS-129518	3090±15	3248-3362	*Sphagnum* spp. stems, *Chamaedaphne calyculata* leaf fragments
328	374.8	UCIAMS-129519	3590±15	3842-3961	*Sphagnum* spp. stems, Ericaceae leaf fragments
376	435.3	UCIAMS-129520	3885±15	4250-4409	*Larix laricina* needles
386	447.9	UCIAMS-135385	3995±20	4421-4519	Bulk peat
IDH					
54	69.7	UCIAMS-135378	140±20	8-278	*Sphagnum* spp. stems
116	118.1	UCIAMS-135379	760±20	670-726	*Sphagnum* spp. stems
137	143.6	UCIAMS-151363	905±20	763-910	*Sphagnum* stems, branches and leaves
191	206.8	UCIAMS-151364	1900±20	1815-1896	*Sphagnum* stems
220	240.7	UCIAMS-135380	2120±20	2007-2150	*Larix laricina* needles, *Myrica gale* and *Chamaedaphne calyculata* leaf fragments, *Sphagnum* spp. stems
286	318.9	UCIAMS-135381	2785±20	2804-2951	*Sphagnum* spp. stems
317	357.0	UCIAMS-151365	3320±20	3479-3607	*Sphagnum* spp. stems
345	390.8	UCIAMS-151366	3480±25	3651-3832	*Sphagnum* spp.stems
394	451.7	UCIAMS-135382	4380±20	4857-5033	*Sphagnum* spp. stems
478	554.3	UCIAMS-135383	4960±25	5612-5737	*Larix laricina* needles and seeds, *Myrica gale* and *Chamaedaphne calyculata* leaf fragments
535	624.1	UCIAMS-123619	6950±25	7699-7839	*Carex* spp. seeds

Table 0.2 Results of ^{210}Pb measurements and CRS modelling on the Baie core.

Sample	Depth (cm)	$^{210}Pb_{tot}$ activity (Bq kg^{-1})	$^{210}Pb_{ex}$ activity (Bq kg^{-1})	CRS ^{210}Pb age (AD)	Uncertainty (a)
Baie 2	1.7	332	316	2010	1
Baie 3	2.9	500	484	2008	1
Baie 4	4.1	257	241	2006	1
Baie 6	6.5	339	323	2003	1
Baie 8	8.9	290	274	2002	1
Baie 10	11	236	221	2001	1
Baie 12	13.4	323	308	1997	1
Baie 14	15.7	358	343	1991	1
Baie 16	17.9	363	347	1987	1
Baie 18	20.3	209	193	1984	2
Baie 20	22.6	268	252	1979	2
Baie 22	24.9	248	232	1974	2
Baie 24	27.3	267	251	1966	2
Baie 26	29.7	237	221	1953	3
Baie 28	32.1	241	225	1921	4
Baie 30	34.5	104	89	1869	8
Baie 32	36.9	32	17		
Baie 34	39.1	16	0		
Baie 36	41.4	15	0		

Table 0.3 Results of ^{210}Pb measurements and CRS modelling on the IDH core.

Sample	Depth (cm)	$^{210}Pb_{tot}$ Activity (Bq kg^{-1})	$^{210}Pb_{ex}$ activity (Bq kg^{-1})	CRS ^{210}Pb age (AD)	Uncertainty (a)
IDH 1	0.8	449	436	2010	1
IDH 2	2.4	480	468	2006	1
IDH 3	3.6	436	423	2001	1
IDH 5	6.0	388	375	1997	1
IDH 7	8.5	373	360	1993	1
IDH 9	10.9	420	408	1990	1
IDH 11	13.3	227	215	1987	1
IDH 13	15.8	334	321	1983	1
IDH 15	18.4	262	249	1980	1
IDH 17	21.1	261	249	1976	2
IDH 19	23.8	193	180	1973	2
IDH 21	26.4	215	202	1968	2
IDH 23	29.1	267	255	1958	3
IDH 25	32.0	175	162	1948	3
IDH 27	34.7	116	104	1938	4
IDH 29	37.5	62	50	1933	4
IDH 31	40.2	53	40	1928	5
IDH 33	42.9	53	40	1920	5
IDH 35	45.6	55	42	1909	6
IDH 37	48.8	53	41	1891	6
IDH 39	51.2	59	47	1865	7
IDH 41	53.6	39	26		
IDH 43	58.6	14	0		
IDH 45	63..2	13	0		

Table 0.1 Nd isotopic data, εNd and $^{206}Pb/^{207}Pb$ for the Baie core.

Sample	Depth (cm)	$^{143}Nd/^{144}Nd$	±2se	εNd	$^{206}Pb/^{207}Pb$	±2se
Baie 3	2.9	0.511924	0.000019	-13.9	1.1657	0.0002
Baie 10	11.0	0.511860	0.000024	-15.2	1.1673	0.0011
Baie 17	19.1	-	-	-	1.1748	0.0006
Baie 22	24.9	-	-	-	1.1792	0.0009
Baie 25	28.5	-	-	-	1.1846	0.0001
Baie 26	29.7	0.511905	0.000006	-14.3	1.1800	0.0009
Baie 26*		0.511912	0.000006	-14.2	1.1803	0.0001
Baie 33	38.0	0.511888	0.000010	-14.6	1.1933	0.0003
Baie 33		*0.511881*	*0.000021*	*-14.8*	*1.1981*	*0.0007*
Baie 36	41.4	0.511932	0.000010	-13.8	1.2057	0.0007
Baie 48	55.7	0.511886	0.000010	-14.7	1.1912	0.0016
Baie 69	81.8	0.511930	0.000008	-13.8	1.1880	0.0005
Baie 74	87.9	0.511894	0.000007	-14.5	-	-
Baie 112	112.5	0.511867	0.000014	-15.0	1.1954	0.0011
Baie 118	119.1	0.511927	0.000007	-13.9	-	-
Baie 119	120.1	0.511911	0.000005	-14.2	-	-
Baie 119		*0.511897*	*0.000008*	*-14.4*	-	-
Baie 120	121.2	0.511921	0.000010	-14.0	-	-
Baie 120		*0.511909*	*0.000007*	*-14.2*	-	-
Baie 128	130.0	0.511941	0.000005	-13.6	1.1936	0.0006
Baie 129	131.1	0.511867	0.000009	-15.0	-	-
Baie 141	144.1	0.511914	0.000005	-14.1	-	-
Baie 148	151.9	0.511949	0.000006	-13.4	-	-
Baie 148		*0.511946*	*0.000007*	*-13.5*	-	-
Baie 150	154.1	-	-	-	1.1979	0.0011
Baie 160	165.1	0.511913	0.000009	-14.1	1.2029	0.0005
Baie 172	178.3	-	-	-	1.2023	0.0001
Baie 174	180.4	-	-	-	1.2011	0.0003
Baie 175	181.5	0.511915	0.000016	-14.1	-	-
Baie 178	184.8	-	-	-	1.1971	0.0006
Baie 201	213.2	0.511954	0.000007	-13.3	1.2098	0.0012
Baie 223	240.3	0.511993	0.000008	-12.6	1.2049	0.0008
Baie 236	257.3	0.511985	0.000012	-12.7	1.2008	0.0008
Baie 262	290.7	0.511956	0.000011	-13.3	1.2134	0.0011
Baie 281	315.1	0.511964	0.000007	-13.2	1.2097	0.0008
Baie 299	338.8	-	-	-	1.2148	0.0006
Baie 340	390.2	-	-	-	1.2082	0.0004
Baie 352	404.9	0.511754	0.000009	-17.9	1.1772	0.0007
Baie 376	435.3	-	-	-	1.1992	0.0003
Baie 383	444.1	0.511494	0.000009	-22.3	1.1562	0.0009
Bottom sed.		0.511544	0.000020	-21.3	1.123	0.0001
Bottom sed.		*0.511554*	*0.000022*	*-21.2*	*1.1316*	*0.0003*
Local soil		0.511729	0.000008	-17.7	1.2058	0.0012
Local soil		*0.511730*	*0.000008*	*-17.7*	*1.2061*	*0.0008*
Beach		0.5116865	0.000009	-19.2	1.1909	0.0009

*Duplicate analysis; italic: replicate analysis

Table 0.2 Nd isotopic data, εNd and $^{206}Pb/^{207}Pb$ for the IDH core.

Sample	Depth (cm)	$^{143}Nd/^{144}Nd$	±2se	εNd	$^{206}Pb/^{207}Pb$	±2se

IDH 7	8.5	0.511919	0.000017	-14.0	1.1668	0.0004
IDH 24	30.5	0.511954	0.000009	-13.3	1.1755	0.0007
IDH 24		*0.511982*	*0.000019*	*-12.8*	*1.1761*	*0.0012*
IDH 27	34.7	0.511971	0.000006	-13.0	1.1785	0.0003
IDH 31	40.2	0.511862	0.000007	-15.1	1.1784	0.0001
IDH 43	56.1	0.511984	0.000009	-12.8	1.1929	0.0001
IDH 52	67.1	0.511905	0.000007	-14.3	1.2533	0.0011
IDH 70	89.0	0.511945	0.000010	-13.5	1.1880	0.0005
IDH 110	111.0	0.512025	0.000010	-12.0	1.1934	0.0004
IDH 137	143.1	0.512015	0.000012	-12.1	1.1965	0.0012
IDH 164	175.1	0.512008	0.000013	-12.3	1.2008	0.0003
IDH 191	206.8	0.512002	0.000008	-12.4	1.2028	0.0010
IDH 236	259.4	0.512021	0.000013	-12.0	1.1982	0.0006
IDH 254	280.5	0.512013	0.000021	-12.2	1.1946	0.0012
IDH 263	290.7	0.511961	0.000014	-13.2	1.2069	0.0003
IDH 299	335.0	0.511999	0.000005	-12.5	1.1944	0.0008
IDH 317	357.0	0.512022	0.000007	-12.0	1.1876	0.0008
IDH 344	389.6	0.512034	0.000006	-11.8	1.2104	0.0005
IDH 371	423.8	0.512015	0.000010	-12.2	1.2062	0.0006
IDH 407	467.3	0.512002	0.000019	-12.4	1.2052	0.0011
IDH 434	500.5	0.511718	0.000011	-17.9	1.2088	0.0009
IDH 470	545.0	0.511664	0.000006	-19.0	1.1846	0.0014
IDH 470		*0.511658*	*0.000006*	*-19.1*	-	-
IDH 493	572.5	0.511556	0.000014	-21.1	1.1223	0.0002
IDH 493		*0.511550*	*0.000014*	*-21.2*	-	-
IDH 532	620.2	0.511563	0.000011	-21.0	1.1283	0.0004
IDH 532		*0.511549*	*0.000046*	*-21.3*	-	-
Bottom sed.		0.511655	0.000007	-19.2	1.1376	0.0008
Beach		0.511658	0.000015	-19.1	1.2143	0.0009

italic: replicate analyses